Soft Matter

# Elasticity and Yielding of Mesophases of Block Copolymers in Water-Oil Mixtures



| | |
|---|---|
| Journal: | *Soft Matter* |
| Manuscript ID | SM-ART-11-2018-002336.R2 |
| Article Type: | Paper |
| Date Submitted by the Author: | 01-May-2019 |
| Complete List of Authors: | Qavi, Sahar; New Mexico State University, Chemical and Materials Engineering<br>Firestone, Millicent; Los Alamos National Laboratory, Materials Physics & Applications<br>Foudazi, Reza; New Mexico State University, Chemical and Materials Engineering |
| | |

# Elasticity and Yielding of Mesophases of Block Copolymers in Water-Oil Mixtures

Sahar Qavi,[a] Millicent A. Firestone,[b] Reza Foudazi*[a]

[a] *Department of Chemical and Materials Engineering, New Mexico State University, Las Cruces, NM 88003*

[b] *Materials Physics & Applications Division, Center for Integrated Nanotechnologies, Los Alamos National Laboratory*

## Abstract

Amphiphilic block copolymers self-assemble at the water/oil interface to form different mesomorphic structures, such as lamellar, micellar cubic, normal hexagonal, and reverse hexagonal. Usually, these structures are polycrystalline and the value of their elastic modulus depends on the average orientation of their constituent's single crystals. We provide a model to predict the elastic modulus and yielding of mesophases from their characteristic length and intermicellar interactions. Shear modulus of each structure is calculated as a function of deformation (strain). Zero-shear modulus, $G_0$, depends on the

* Corresponding author, email: rfoudazi@nmsu.edu, Tel: (+1) 575 646 3691

inverse of intermicellar distance with a power law model. The power law index for each structure is approximately $n$+2 where $n$ is the degree of confinement in the mesophase: 1 for lamellar, 2 for both normal and reverse hexagonal, and 3 for micellar cubic structure. Rheological properties of different mesophases of Pluronic P84 in the presence of water and p-xylene are used as a case study. The model is found to be in good agreement with experimental data in the linear viscoelastic region. When compared to experimental data, the yield strain value from the model is one order of magnitude higher than the limit of the linear viscoelastic regime and close to the strain at cross-over point of storage and loss moduli. Frequency sweep measurements are done to characterize the relaxation and cooperative model behaviors of each mesophase structure.

## 1. Introduction

In the presence of selective solvents, amphiphilic block copolymers self-assemble and form different mesomorphic structures known as mesophases. Examples of mesophase structures are micellar cubic, lamellar, normal and reverse hexagonal.[1–4] A rich structural polymorphism has been observed in ternary water/oil/block copolymer systems, with the

block copolymer self-assembly forming micro-domains with spherical, cylindrical, or lamellar geometry, discrete or interconnected topology, and liquid-crystalline organization.[5–8] These polycrystalline systems consist of randomly oriented single crystals and can be characterized as an isotropic system. Mesophases of block copolymer solutions are thermodynamically stable systems, where each block of copolymer energetically minimizes unfavorable interactions with its poor solvent. In this context, mesophases are comparable to microemulsions, where thermodynamics plays the dominant role in the stability of the system rather than interfacial tension.

Mesophases have been utilized in a broad range of applications, such as pharmaceutical and biomedical applications[9–12], and as templates for mesoporous material synthesis for hydrogels,[13–15] separation processes,[16–19] and adsorption applications.[20,21] Rheological behavior of mesophases varies with structure and has an important role not only in their applications in industry, but also from a theoretical point of view.

While there are several rheological studies on the self-assembly of block copolymer melts,[22–24] low molecular weight surfactant solutions,[25–29] and flow-induced behavior and

rheology of block copolymers in single solvents,[30–34] less work has been reported on the rheology of block copolymers in the presence of two solvents (ternary system).[35,36] Additionally, the elastic modulus of mesophases is highly dependent on their structure. For instance, lamellar mesophases are shown to have an elastic modulus of at least one order of magnitude lower when compared to hexagonal systems.[27,35–37] The size of lattice parameter and intermicellar interactions within the mesophase are two important factors to be considered when evaluating each structure.

Since mesophases are crystalline, estimation of their elastic constants can give us a general picture of their mechanical properties. Several simulation studies have been done to estimate the elastic constants of crystalline and amorphous polymers.[38–40] For instance, Van Workum and de Pablo[38,40] developed a method to calculate the elastic constants of face-centered cubic (FCC) crystals at different temperatures, where the bulk elastic constants are calculated in terms of stress fluctuations. Although simulation techniques are invaluable in evaluating the mechanical properties of crystalline materials,

no analytical model, to the best of our knowledge, has been proposed to estimate the average elastic modulus of a self-assembled mesophase based on its structure.

In polycrystalline systems of metals, effective isotropic elastic constants can be derived from averaging elastic constants of their constituent single crystal grains.[41–44] Depending on the crystalline structure of the unit cell, independent elements in the elasticity tensor are determined. Then, an averaging method is applied to calculate the tensile and/or shear modulus of the polycrystalline metal. We contend this method can be utilized for liquid crystalline mesophases. In the current work, we use this approach to model the elastic shear modulus and yielding behavior of different polymeric mesophases. Additionally, we show how the shear modulus of different mesophase structures change by intermicellar distance and micelle size. Rheological measurements in the linear viscoelastic regime are used to validate the model predictions. Considering the solid-like behavior of mesophases,[45–47] comparing the estimated elastic modulus with the G' in the linear viscoelastic region is appropriate.

In the following sections, we first present the model to predict the shear elastic modulus of three different mesophase systems, namely micellar cubic, lamellar, and reverse/normal hexagonal, based on their intermicellar interactions and lattice parameter. Next, we present the preparation and characterization of our experimental systems. Then, we discuss the results by comparing the model and experimental data. Finally, we conclude with summarizing the key findings.

## 2. Model

From the generalized Hookes's law, $\sigma = C\,\varepsilon$, where, $\sigma$ and $\varepsilon$ are stress and strain tensors, respectively. $C$ is known as the elasticity tensor, and for an isotropic material has 21 independent elements.[48] Single crystals are not isotropic and the number of independent elements in their elasticity tensor depends on the crystal structure and its symmetry. For the cubic and hexagonal structures, the non-zero components of the elasticity matrix can be expressed as follows:[48]

$$C_C = \begin{bmatrix} c_{11} & c_{12} & c_{12} & & & \\ c_{12} & c_{11} & c_{12} & & & \\ c_{12} & c_{12} & c_{11} & & & \\ & & & c_{44} & & \\ & & & & c_{44} & \\ & & & & & c_{44} \end{bmatrix} \quad (1)$$

$$C_H = \begin{bmatrix} c_{11} & c_{12} & c_{13} & & & \\ c_{12} & c_{11} & c_{13} & & & \\ c_{13} & c_{13} & c_{33} & & & \\ & & & c_{44} & & \\ & & & & c_{44} & \\ & & & & & \frac{c_{11}-c_{12}}{2} \end{bmatrix} \quad (2)$$

where $C_C$ and $C_H$ are elasticity matrices for the cubic and hexagonal systems, respectively. There are 3 independent second order elastic constants (SOECs) for the cubic structure, while hexagonal structure has five SOECs.

Voigt averaging procedure is commonly used for estimating elastic constants of polycrystals. In this method, we assume that all single crystals are in the same state of strain.[41,49] Voigt-average shear modulus of cubic ($G_{V,C}$) and hexagonal ($G_{V,\ H}$) polycrystals are defined as follows: [42,44]

$$G_{V,C} = \frac{(c_{11} - c_{12} + 3c_{44})}{5} \quad (3)$$

$$G_{V,\ H} = \frac{A' - B' + 3C'}{5} \quad (4)$$

where,

$$A' = \frac{1}{3}(2c_{11} + c_{33}) \quad (4.a)$$

$$B' = \frac{1}{3}(c_{11} + c_{12} + c_{13}) \quad (4.b)$$

$$C' = \frac{1}{3}(2c_{44} + \frac{c_{11} - c_{12}}{2}) \quad (4.c)$$

To calculate the elastic constant elements in equations (1) and (2), we consider three systems of spherical micelles in micellar cubic mesophases, cylindrical micelles in hexagonal mesophases, and planar micelles in lamellar mesophases. Van der Waals forces are assumed as the primary interaction between micelles. Similar to microemulsions, mesophases are thermodynamically stable systems, where the interfacial tension between oil and water becomes zero[50–52] and leads to the spontaneous formation of mesophases. Consequently, the interfacial tension effect on the elastic behavior of the mesophases is negligible.

For each system, we consider a single crystal undergoing deformation in the presence of van der Waals forces between nearest neighbors. We assume micelle size does not

change under deformation and only their distances change. This assumption is rational as micelles primarily consist of block copolymer chains and the force acting between two block copolymer molecules in a short range (in the order of a few angstroms) is much higher than the force between two micelles in a longer range (in the order of a few nanometers). In other words, the deformation of the unit cell can hardly separate the adjacent block copolymer molecules to change the size of micelles. Net force of the system after deformation is calculated by subtracting the sum of the forces before deformation from the sum of the forces after deformation. It has been shown that the second derivative of free energy, $U$, with respect to strain ($\gamma$) is proportional to the shear modulus, $G$, as $G \propto \frac{\partial^2 U}{\partial \gamma^2}$.[53] Force has a direct relationship with energy; therefore, we can use the strain derivative of net force as a measure of elastic constants.

In the following sub-sections, we provide a model for each mesophase system.

### 2.1. Micellar cubic mesophases

For the sake of simplicity, we assume a simple cubic system, a cube with a lattice parameter, $a$, where eight spheres with a diameter of $R_C$ are located in each corner (Figure 1). Each micelle consists of an oil phase, water phase, and a Pluronic block copolymer

that acts as a surfactant at the interface. Upon deformation in direction 1, distance $a$ changes to $b$ and $c$, where $b < a$ and $c > a$.

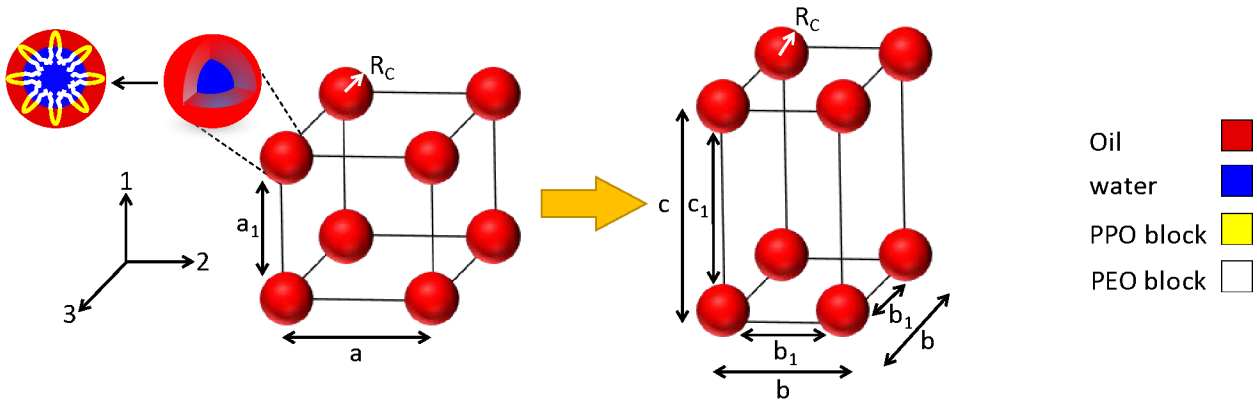


Figure 1. Schematic representation of a micellar cubic mesophase undergoing deformation in direction 1. The legend shows different components in each spherical micelle.

Van der Waals forces, $F_C$, between two identical spheres with distance $a_1$ is:[54]

$$F_C = \frac{-A_H R_C}{12 {a_1}^2} \quad (5)$$

where $A_H$ in the Hamaker constant and $R_C$ is the radius of each sphere. Before applying deformation, 12 van der Waals forces ($F_{C,0}$) between nearest neighbors can be considered. After deformation, the interaction forces ($F_{C,1}$) would be:

$$F_{C,1} = 8\frac{-A_H R_C}{12 {b_1}^2} + 4\frac{-A_H R_C}{12 {c_1}^2} \quad (6)$$

where $b_1$ and $c_1$ are the new distances between spheres in directions $2$ and $1$, respectively. Strain in each direction can be defined as the ratio of the change in length to the initial length.[55] Therefore:

$$\varepsilon_{C1} = \frac{c-a}{a} \quad (7a)$$

$$\varepsilon_{C2} = \varepsilon_{C3} = \frac{b-a}{a} \quad (7b)$$

where $\varepsilon_{C1}$, $\varepsilon_{C2}$, and $\varepsilon_{C3}$ are the strains in directions $1$, $2$, and $3$, respectively. Considering no change in the spheres' size and the incompressibility assumption:

$$c_1 = a\varepsilon_{C1} + a_1 \quad (8)$$

$$b_1 = a\varepsilon_{C2} + a_1 \quad (9)$$

$$(a_1 + 2R_C)^3 = (b_1 + 2R_C)^2(c_1 + 2R_C) \quad (10)$$

where $a_1 = a - 2R_C$ , $b_1 = b - 2R_C$, and $c_1 = c - 2R_C$.

Tensile elastic constants are defined as follow:

$$C_{C11} = \frac{\partial^2 \Delta F_C}{\partial \varepsilon_{C1}^2} \quad (11a)$$

$$C_{C12} = \frac{\partial^2 \Delta F_C}{\partial \varepsilon_{C1} \partial \varepsilon_{C2}} \quad (11b)$$

where $\Delta F_C$ is the change in interaction forces after deformation. Detailed derivation of the equations can be found in the Electronic Supplementary Information (ESI). Additionally, from the theory of linear elasticity, the shear strain can be determined from tensile strains as $\gamma_{C12} = \frac{\varepsilon_{C1} - \varepsilon_{C2}}{2}$. Therefore, the shear elastic constant is obtained (refer to ESI). Having all the independent constants in the elasticity matrix in equation (1), we use the Voigt average, equation (3), to calculate the shear modulus of micellar cubic mesophases.

Critical molecular weight entanglement ($M_c$) for polyethylene oxide (PEO) and polypropylene oxide (PPO) are 10,000 g/mol and 7000 g/mol, respectively.[56,57] As will be discussed in the experimental section, we use Pluronic P84 block copolymer in samples, which has a molecular weight well below $M_c$. Therefore, block copolymers are not entangled in the system. Additionally, the radius of gyration of Pluronic P84 block copolymer is approximately 17 Å,[8] which is smaller than the domain size of the micelles. Thus, chains do not bridge across the hydrophilic and hydrophobic domains (shown as

blue and red areas in the figures, respectively), which is valid for all studied structures in this work.

### 2.2. Lamellar mesophases

Lamellar system can be assumed to behave like a cubic system in which parallel plates are aligned in direction $2$ and their unit cell size is $d$ (Figure 2). Upon deformation in direction $1$, the distance $d$ changes to $d_1$. The extension in direction 1 leads to a compression deformation in direction 2 from $d$ to $d_2$.

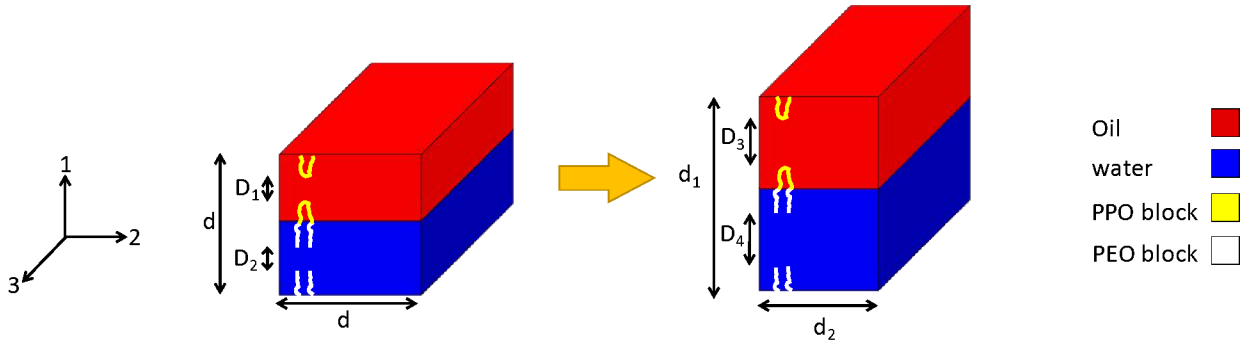


Figure 2. Schematic representation of a lamellar mesophase undergoing deformation in direction 1. The legend shows different components in each micelle.

Van der Waals forces, $F_{L,0}$, between two identical plates with distance $D$ is:[54]

$$F_{L,0} = \frac{-A_H}{6\pi {D_1}^3} + \frac{-A_H}{6\pi {D_2}^3} \quad (12)$$

After deformation, the interaction forces would be:

$$F_{L,1} = \frac{-A_H}{6\pi {D_3}^3} + \frac{-A_H}{6\pi {D_4}^3} \quad (13)$$

Intermicellar distances ($D_1$, $D_2$, $D_3$, and $D_4$ ) are shown in Figure 2 and defined in the ESI. Strain in directions $1$ and $2$ are given in equations (14a) and (14b). Iso-strain condition is assumed in direction $3$ for simplicity.

$$\varepsilon_{L1} = \frac{d_1 - d}{d} \quad (14a)$$

$$\varepsilon_{L2} = \frac{d_2 - d}{d} \quad (14b)$$

$$\varepsilon_{L3} = 0 \quad (14c)$$

Considering the incompressibility assumption, we have $d^2 = d_1 d_2$. Detailed derivation of the equations is shown in the ESI. Having all the independent constants in the elasticity matrix in equation (1), we use the Voigt average, equation (3), to calculate the shear modulus of lamellar mesophases.

### 2.3. Hexagonal mesophases

We assume a hexagonally packed structure with lattice parameter $h$, where 6 cylindrical micelles with diameter of $R_H$, are located in the corners with one located at the center of the hexagon (Figure 3). Upon deformation in direction $1$, the hexagon becomes deformed and the distance $h$ changes to $l$ and $x$, where $x < h$ and $l > h$. For the sake of simplicity, we assume the angles remain constant at 120°. It should be noted that without this assumption, the geometrical relationships become too complicated to provide an analytical solution. In the following sections, we will show that this assumption still offers satisfactory agreement between the model and experimental data. No deformation in the length of cylinders and direction $3$ is assumed. Additionally, only the interaction of nearest neighbors is considered.

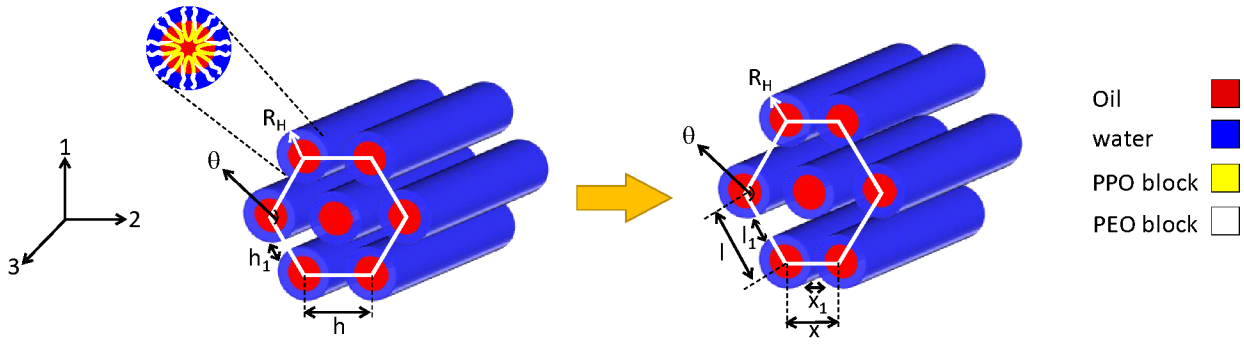


Figure 3. Schematic representation of a hexagonal mesophase undergoing deformation in direction 1. The legend shows different components in each cylindrical micelle.

Van der Waals forces, $F_H$, between two identical cylinders[54] with distance $D$ is $F_H = \frac{-A_H\sqrt{R_H/2}}{8\sqrt{2}D^{5/2}}$, where $R_H$ is the radius of each cylinder. The derivation of the elastic constants form the change in free energy under deformation which contains the square root of negative values, resulting in complex numbers. To avoid this, we have used $D^{13/5}$ in the van der Waals interaction between cylinders, which is approximately equal to $D^{2.5}$ and does not result in complex numbers. Before applying deformation, 12 van der Waals interactions can be considered as follows:

$$F_{H,0} = 4\frac{-A_H\sqrt{R_H/2}}{8\sqrt{2}\,{h_1}^{13/5}} + 8\left(\frac{-A_H\sqrt{R_H/2}}{8\sqrt{2}\,{h_1}^{13/5}}cos\,\theta/_2 + \frac{-A_H\sqrt{R_H/2}}{8\sqrt{2}\,{h_1}^{13/5}}sin\,\theta/_2\right) \quad (15)$$

where $h_1$ is the distance between cylindrical micelles in hexagonal mesophases. In a perfect hexagon, $\theta = 120°$; therefore:

$$F_{H,0} = (8 + 4\sqrt{3})\frac{-A_H\sqrt{R_H/2}}{8\sqrt{2}\,{h_1}^{13/5}} \quad (16)$$

After deformation, the interaction forces would be:

$$F_{H,1} = 2\frac{-A_H\sqrt{R_H/2}}{8\sqrt{2}\,{x_1}^{13/5}} + 8\left(\frac{-A_H\sqrt{R_H/2}}{8\sqrt{2}\,{l_1}^{13/5}}cos\theta + \frac{-A_H\sqrt{R_H/2}}{8\sqrt{2}\,{l_1}^{13/5}}sin\theta\right) + 2\frac{-A_H\sqrt{R_H/2}}{8\sqrt{2}\,(\frac{x+l}{2} - 2R)^{13/5}} \quad (17)$$

where $x_1$ and $l_1$ are the new distances between cylinders. Strain in each direction can be defined as follows:

$$\varepsilon_{H1} = \frac{lsin\theta - \frac{\sqrt{3}}{2}h}{\frac{\sqrt{3}}{2}h} \quad (18a)$$

$$\varepsilon_{H2} = \frac{x-h}{h} \quad (18b)$$

$$\varepsilon_{H3} = 0 \quad (18c)$$

As mentioned previously, we have assumed the angle $\theta$ remains fixed during deformation and only the distances between cylinders change in the hexagonal arrangement. Thus, considering no change in the cylinders and the incompressibility assumption:

$$\frac{3}{2}h^2 = l\left(x + \frac{l}{2}\right) \quad (19)$$

$$l_1 = h\varepsilon_{H1} + h_1 \quad (20)$$

$$x_1 = h\varepsilon_{H2} + h_1 \quad (21)$$

Detailed derivations of the tensile elastic constants are shown in the ESI. In a hexagonal packed system, $C_{H66} = \frac{C_{H11} - C_{H12}}{2}$.[48] Thus, having all the independent constants in the elasticity matrix in equation (2), we use the Voigt average, equation (4), to calculate the elasticity of hexagonal mesophases.

## 3. Experimental Section

### 3.1. Materials

Poly(ethylene oxide)$_{19}$-poly(propylene oxide)$_{43}$-poly(ethylene oxide)$_{19}$ triblock copolymer, known as Pluronic P84 ($M_w$=4200 g/mol), is kindly provided by BASF. Deionized (DI) water and p-xylene (Sigma-Aldrich) are used as selective solvents for PEO and PPO blocks, respectively.

### 3.2. Mesophase Preparation

Pluronic P84, DI water, and p-xylene are mixed in a glass vial through centrifugation. In this process, samples are repeatedly centrifuged (2000 rpm) at alternative directions until

a transparent mesophase is obtained. We select a constant concentration of Pluronic P84 in which, by changing water/p-xylene ratio, different mesophase structures – micellar cubic, lamellar, normal hexagonal, and reverse hexagonal – are obtained. Composition shown in Table 1 are chosen based on the ternary phase diagram of the system.[8]

Table 1. Formulations of samples used in this study.

| P84/water/p-xylene (wt%) | Mesophase type |
|---|---|
| 50/35/15 | lamellar ($L_\alpha$) |
| 50/47.5/2.5 | normal hexagonal ($H_1$) |
| 50/20/30 | reverse hexagonal ($H_2$) |
| 50/10/40 | micellar cubic (BCC) |

### 3.3.Small Angle X-ray Scattering (SAXS) Measurements

Mesophase samples are loaded into quartz capillaries with a nominal diameter of 1.5 mm (Charles Supper Company, Natick, MA). The capillary tubes are then sealed using

Critoseal tube sealant and epoxy glue (JB Weld). SAXS measurements are performed on a Bruker Nanostar System with a monochromated Cu Kα radiation source. The beam center and sample-to-detector distance are determined using silver behenate.

### 3.4. Rheological Measurements

Rheological tests are carried out on a stress-controlled Discovery Hybrid Rheometer (DHR-3) from TA Instruments (New Castle, DE). A 20 mm cross-hatched parallel plate geometry with 1 mm gap is used for measurements. The cross-hatched geometry is used to avoid probable wall slip of mesophases during measurements. The temperature during the tests is controlled at 25±0.1 °C by a peltier plate system. Small amplitude oscillatory shear tests are done at a fixed strain of 0.5% in the linear viscoelastic region (verified by amplitude sweep tests). Isothermal dynamic amplitude sweep is carried out at the fixed frequency of 10 rad/s.

## 4. Results and Discussion

### 4.1. SAXS Analysis

One dimensional (1D) SAXS data obtained for different mesophases are shown in Figure 4. Relative peak positions ($q/q^*$) is used to determine the structure of each sample.

Lamellar structures show 1:2:3:4… relative peak positions, hexagonal structures have 1:√3:2:√7:3… relative peak positions, and micellar cubic (body centered cubic, BCC) structures have relative peak positions of 1:√2:2:√6, were $q$ is the scattering vector and $q^*$ is the principal peak in each curve.

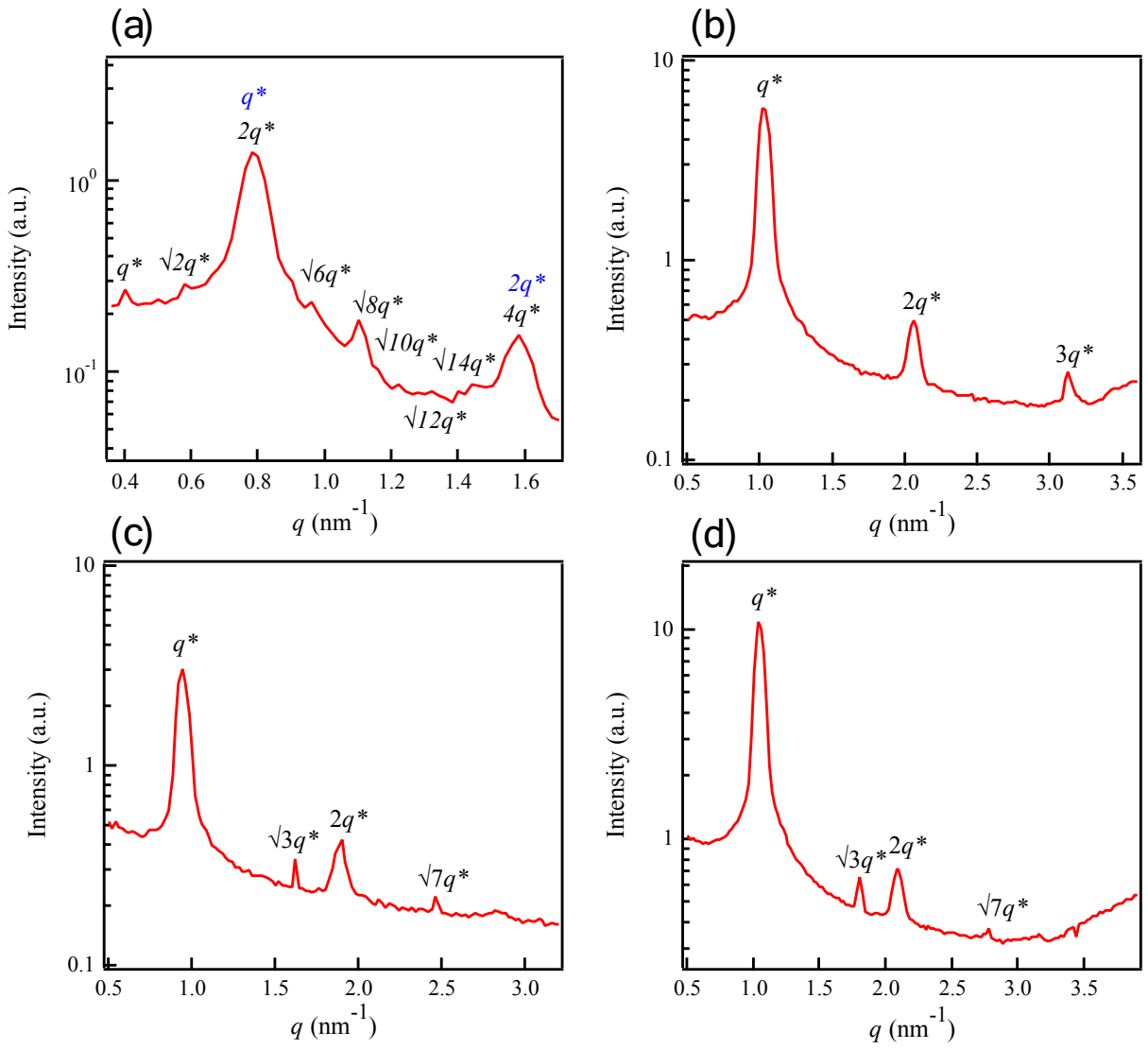


Figure 4. Radially averaged I(q) from SAXS scattering of mesophase systems containing Pluronic P84/water/p-xylene: (a) micellar cubic with 50/10/40 composition, (b) lamellar with 50/35/15 composition, (c) normal hexagonal with 50/47.5/2.5 composition, and (d) reverse hexagonal 50/20/30 composition.

It should be noted that the pattern shown in Figure 4a might have mixed phases, where the peaks shown in black are cubic, and the ones indexed in blue are lamellar. From the

phase diagram of the system[8] and the rheological measurements that will be presented in the following sections, we can conclude that the composition has mainly a cubic phase (BCC from *Im3m* space group).

From the SAXS scattering profiles and using Bragg's law, lattice parameter for each mesophase, radius of spheres and cylinders in micellar cubic and hexagonal mesophases, respectively, and the distance between micelles are calculated. These parameters are schematically shown in Figure 5. From Bragg's law, $2d\sin\varphi = n\lambda$, where $\lambda$ is the X-ray wavelength, $\varphi$ is the scattering angle, $n$ is the order of reflection (taken as 1 for the principal scattering vector, $q^*$), and $d$ is the lattice parameter.[58] The magnitude of the scattering vector, $q$, is $q = \frac{4\pi\sin\varphi}{\lambda}$. For a lamellar structure, the lattice parameter, $d_L$, also known as the lamellar periodicity, is defined as $d_L = \frac{2\pi}{q^*}$. For hexagonal mesophases, the lattice parameter, $d_H$, which is equal to the distance between the centers of adjacent cylinders, can be calculated as $d_H = \frac{4\pi}{\sqrt{3}q^*}$.[8] In the case of the micellar cubic mesophase, the first six Bragg peaks identified from SAXS data in Figure 4a are indexed as 110, 200,

211, 220, 310, and 222.[53] The slope of the line passing through the origin of the $\frac{1}{d_{hlk}}$ versus $(h^2 + l^2 + k^2)^{1/2}$, is equal to the reciprocal of the lattice parameter, $\frac{1}{d_c}$.[8,45]

Apolar domain volume fraction, $f$, is defined as the volume fraction of p-xylene and the PPO block; the polar domain volume fraction, $1 - f$, is the volume fraction of water and the PEO block. Thus, the thickness of the polar and apolar domains in lamellar mesophases and the radius of the polar and apolar domains in micellar cubic and hexagonal mesophases are determined and shown in Table 2. We have used these parameters in the model to plot the estimated shear modulus versus deformation.[8,59]

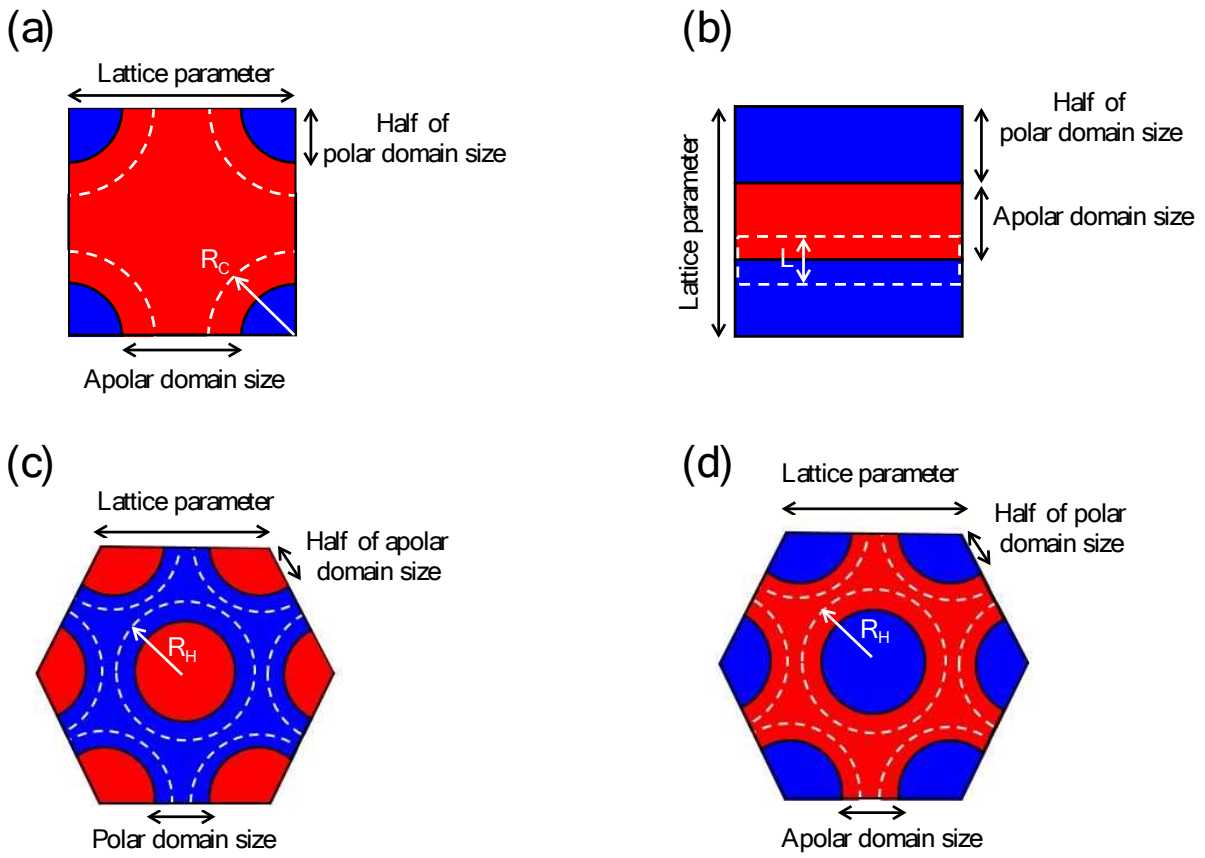


Figure 5. Schematic representation of the lattice parameter, polar domain, and apolar domain in (a) micellar cubic, (b) lamellar, (c) normal hexagonal, and (d) reverse hexagonal mesophases. Dashed lines show the micelle size in (a) BCC as $R_C$, (b) lamellar as L, and (c,d) hexagonal systems as $R_H$.

Table 2. Calculated parameters for micellar cubic, lamellar, normal hexagonal and reverse hexagonal mesophases from SAXS.

| Mesophase structure | Lattice parameter (nm) | $f$ | Polar domain size (nm) | Apolar domain size (nm) | $R_C$ or $R_H$ (nm) | Intermicellar distance (nm) |
|---|---|---|---|---|---|---|
| BCC | 7.9 | 0.72 | 6.56 | 1.34 | 3.42 | 1.06 |
| $L_\alpha$ | 6.0 | 0.46 | 3.24 | 2.76 | NA | 1.92,2.64* |
| $H_1$ | 7.6 | 0.33 | 5.31 | 2.29 | 1.15 | 5.3 |

| | | | | | | |
|---|---|---|---|---|---|---|
| $H_2$ | 7.0 | 0.62 | 4.11 | 2.89 | 2.05 | 2.9 |

* The two numbers stand for intermicellar distance in apolar and polar domains, respectively.

### 4.2.Rheological Analyses

Since mesophases have gel-like behavior,[45,46] rheology is a sufficient tool to measure the modulus and yielding behavior. Consequently, rheological experiments are performed in the linear viscoelastic region. It should be noted that since the model predicts the linear response of mesophases, we have only done oscillatory tests in the linear viscoelastic regime to validate the model. We have done comprehensive large amplitude oscillatory shear (LAOS) tests on the samples that are out of scope of this work. However, we have seen a hysteresis (the area in the closed loop graph of stress versus strain) in the Lissajous plots that only appears at high amplitudes of oscillatory deformation (non-linear regime). In fact, high amplitude deformations can result in the alignment and or change in structure of mesophases,[60,61] which we believe are out of the scope of the current work. Amplitude sweep tests are done to determine the linear viscoelastic region of each mesophase. Experimental results for micellar cubic, lamellar, reverse hexagonal, and normal hexagonal structures, along with the developed model in the previous section, are

shown in Figure 6. Data presented in Table 2 are used as the model parameters. The Hamaker constant ($A_H$) values for hydrocarbons and water are approximately 0.5 × $10^{-19}$ J and 1.5 × $10^{-19}$ J, respectively.[62] For lamellar and normal hexagonal systems, the Hamaker constant is considered as 1.5 × $10^{-19}$ J, while its value is assumed to be 0.5 × $10^{-19}$ J for reverse hexagonal and reverse BCC structures. It should be noted that any variation in the Hamaker constant linearly changes the values of elastic constants.

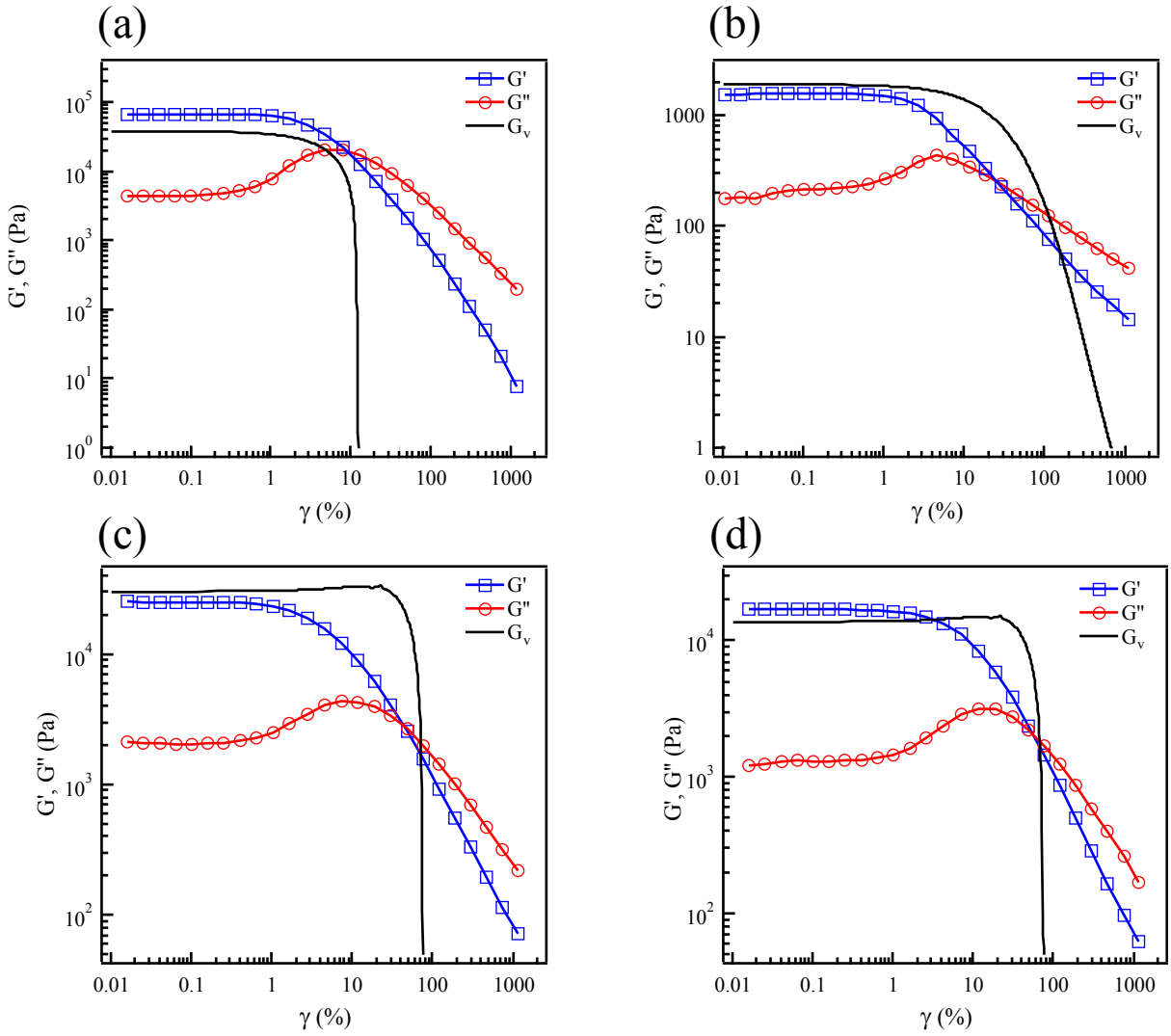


Figure 6. Storage modulus, G', and loss modulus, G", versus strain obtained through amplitude sweep experiments on (a) micellar cubic, (b) lamellar, (c) normal hexagonal and (d) reverse hexagonal mesophases of Pluronic P84/water/p-xylene with 50/10/40, 50/35/15, 50/47.5/2.5, and 50/20/30 compositions, respectively. Solid lines are the estimated shear modulus from the models developed for each mesophase structure.

Calculated shear elastic modulus from the model (solid lines in Figure 6) is in very good agreement with the value of elastic modulus from rheological experiments, confirming that

the interactions between micelles within randomly orientated grains of liquid crystals determines the value of the shear modulus in mosophases. The micellar cubic mesophase shows the highest elastic modulus among other mesophases, which is due to its higher symmetry and higher coordination number (the number of the nearest neighbors). Values of elastic modulus of micellar cubic is in the same order of magnitude with the one of the hard gel cubic structures.[63] The normal hexagonal mesophase shows slightly higher elastic modulus compared to the reverse one.[64] Based on the proposed model, we can explain the observed difference based on the distance between cylindrical micelles in normal and reverse hexagonal systems in this study, originated from different compositions and lattice parameter sizes in each system (Table 2). In addition, the value of the Hamaker constant in the normal hexagonal case is higher than that of the reverse hexagonal mesophase, having a higher contribution to the elastic constants for the normal phase. The lamellar mesophase shows at least one order of magnitude lower elastic modulus compared to micellar cubic and hexagonal mesophases, in agreement with our experimental data and the literature.[27,35–37]

The point where the elastic modulus (G') starts to decrease with strain is the threshold of non-linear viscoelastic region, $\gamma_{LVE}$, and can be defined as the yield point.[65] Based on the experimental data, all mesophase structures show the same trend in the amplitude sweep curve. This trend is known as type III non-linear behavior which is evident by a weak strain overshoot and a local maximum in loss modulus (G"). Polymer solutions and highly concentrated emulsions (HCE) have the same behavior.[63,66–68] We suggest that the rearrangement of micellar structures in mesophases are the main reasons for observing type III behavior.[69–71] An alternative definition for yield strain is the crossover of G' and G", $\gamma_{y,G'=G"}$, beyond which the loss modulus (as a measure of energy dissipation) is dominant. The experimental values of yield strain ($\gamma_{LVE}$ and $\gamma_{y,G'=G"}$), based on two different definitions provided, are extracted from rheological data as shown in Table 3. In addition, from our model, we can estimate the yield strain ($\gamma_{y,model}$) as the point where $G_v$ decreases with strain. Ideally, we expect to have similar values for $\gamma_{LVE}$ and $\gamma_{y,model}$. However, the data in Table 3 show that our model overestimates the yield strain point. We attribute this deviation from experimental data to the simplifying assumptions. For

instance, while grain boundaries contribute to the yielding process, our model does not consider them. Interestingly, $\gamma_{y,G'=G''}$ is in the same order of magnitude with the $\gamma_{y,model}$.

Table 3. Calculated values of yield strain for different mesophases from model and experimental data.

| Mesophase structure | $\gamma_{LVE}$ (%) | $\gamma_{y,G'=G''}$ (%) | $\gamma_{y,model}$ (%) |
|---|---|---|---|
| BCC | 1.00 | 8.0 | 8.6 |
| $L_\alpha$ | 1.6 | 28.2 | 12.0 |
| $H_1$ | 1.1 | 47.7 | 28.5 |
| $H_2$ | 1.0 | 48.2 | 25.0 |

Our model suggests that the shear modulus is highly dependent on the distance between interacting micelles, and consequently the lattice parameter of each mesophase, as shown in Figure 7. For each mesophase system, we have plotted the estimated zero-shear modulus ($G_0$, modulus at very low deformation, i.e. 0.01%) from the model as a function of reciprocal intermicellar distance ($\frac{1}{D}$), considering the lattice parameter changes in the range of 2-50 nm, a domain range that can practically be observed in these systems. The results indicate that $G_0$ dependency to the intermicellar distance increases

as the distance increases. A power law equation, $G_0 = A_0(\frac{1}{D})^m$, is used to fit the data, where $A_0$ and $m$ are the model parameters (listed in Table 4 for different mesophases). The power law index for each structure is approximately $m \approx n + 2$, where $n$ is the degree of confinement in each system. In other words, micellar cubic mesopahses have three-dimensional confinement and $m \approx 3 + 2 = 5$, lamellar mesophases with one degree of confinement, have $m \approx 1 + 2 = 3$, and both normal and reverse hexagonal systems with two-dimensional confinement show $m \approx 2 + 2 = 4$.

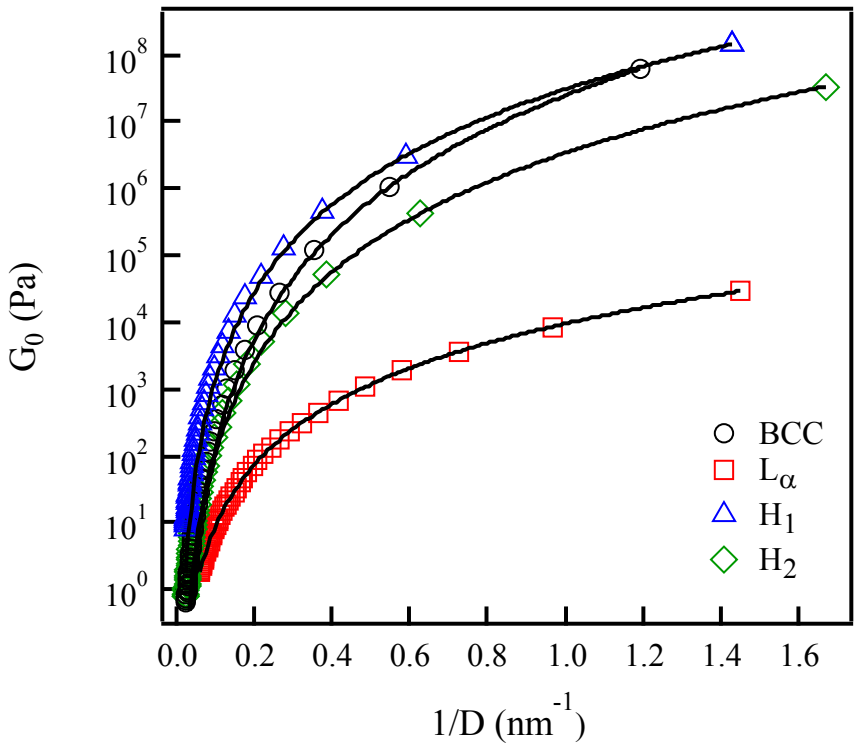

Figure 7. Calculated zero-shear modulus as a function of inverse intermicellar distance (1/D) for micellar cubic, lamellar, normal hexagonal, and reverse hexagonal systems. The solid lines are a power law fit to the data.

Dependency of the calculated zero-shear modulus on micelle size is different from that of micellar distance. At a constant intermicellar distance, $G_0$ is plotted against micelle size in Figure 8. Micelle size is defined as $R_C$ for cubic, L for lamellar, and $R_H$ for normal and reverse hexagonal systems (Figure 5). For the lamellar system, $G_0$ is independent of micelle size as expected; for micellar cubic mesophase structures, it is a power law function of micelle size ($G_0 = A_C {R_c}^{n_C}$); for normal and reverse hexagonal systems, $G_0$ is approximately an exponential function of micelle size ($G_0 = A_H e^{-n_H R_H}$). For BCC system, the power law index is constant at three different intermicellar distances ($n_C = 1.6$) and only the pre-power parameter changes. In normal and reverse hexagonal mesophases, both the pre-exponential parameter and exponential index are a function of intermicellar distance. At a constant intermicellar distance, the index in both normal and reverse hexagonal systems are the same. Model parameters are summarized in Table 4.

Table 4. The power law model parameters for calculated zero-shear modulus dependency to the inverse of intermicellar distance and the power law and exponential model parameters for calculated zero-shear modulus dependency to micelle size in different mesophase systems.

| Structure | $A_0$ | $m$ | Intermicellar distance (nm) | $A_C$ or $A_H$ | $n_C$ or $n_H$ |
|---|---|---|---|---|---|
| BCC | $2.6 \times 10^7$ | 5.2 | 2 | 623 | 1.8 |
| | | | 5 | 18 | 1.8 |
| | | | 8 | 4 | 1.8 |
| $L_\alpha$ | 265 | 3.0 | 2 | 41879 | 0 |
| | | | 5 | 2680.3 | 0 |
| | | | 8 | 654.4 | 0 |
| $H_1$ | $3.2 \times 10^7$ | 4.3 | 2 | $1.2 \times 10^6$ | 0.5 |
| | | | 5 | $2.1 \times 10^4$ | 0.4 |
| | | | 8 | $5.3 \times 10^3$ | 0.25 |

| | | | | | |
|---|---|---|---|---|---|
| | | | 2 | $6.6\times10^{4}$ | 0.5 |
| $H_2$ | $3.5\times10^{6}$ | 4.4 | 5 | $1.6\times10^{3}$ | 0.4 |
| | | | 8 | 325 | 0.25 |

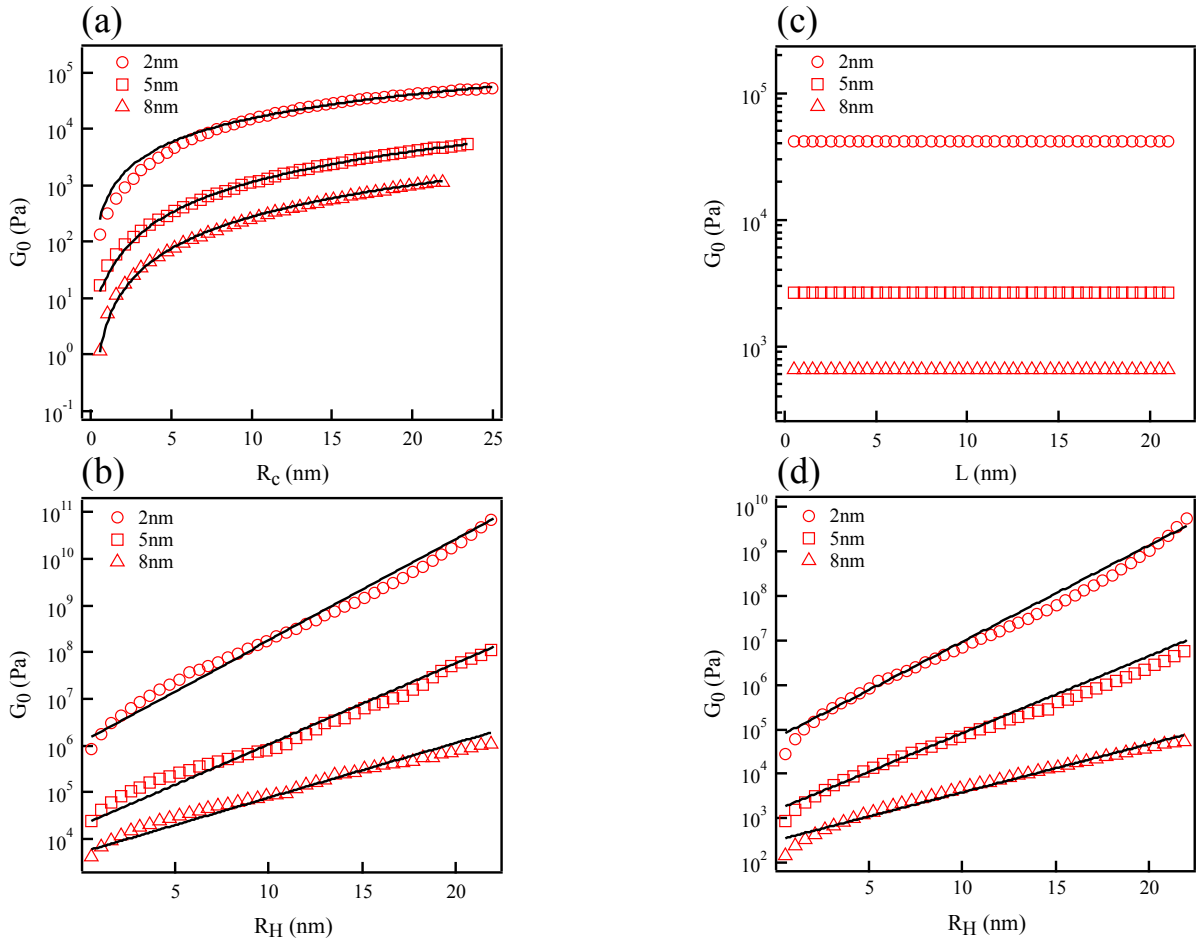


Figure 8. Calculated zero-shear modulus as a function of micelle size for (a) micellar cubic, (b) lamellar, (c) normal hexagonal, and (d) reverse hexagonal systems at 3 constant intermicellar distances (values in the legends). Solid lines are the power law (for BCC) and exponential (for $H_1$ and $H_2$) fits to the data.

After determining the extent of linear viscoelastic region for each mesophase, a dynamic frequency sweep experiment is done on samples in the linear regime to measure the linear viscoelastic properties of the mesophases. As seen in Figure 9, G' is higher than G" in all frequency ranges (0.06-600 rad/s) for all mesophases, which implies the solid-like behavior of the samples. G' is nearly frequency-independent with a subtle increase with increasing frequency. G' of the reverse hexagonal mesophase is slightly lower than that of its normal counterpart, which could be due to the difference in micelle size and intermicellar distance, as explained in the previous paragraphs. All samples are in the rubbery-plateau region of the universal frequency sweep curve of viscoelastic materials, where G' is higher than G" and no G'-G" crossover is seen in frequency sweep data, indicating high structural relaxation times of mesophases. All mesophases show shear-thinning behavior as their complex viscosity ($\eta^*$) decreases with increasing frequency.

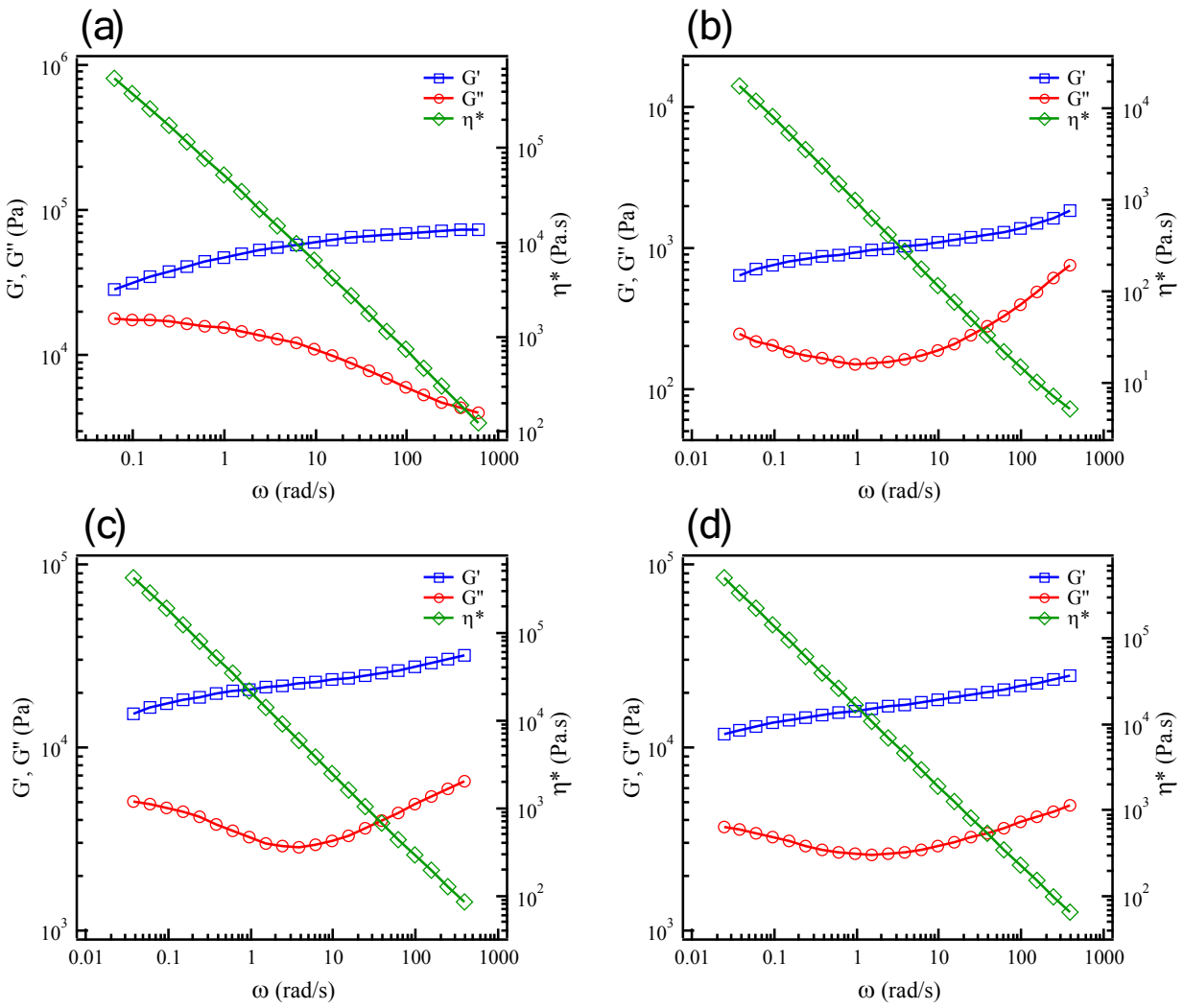


Figure 9. Storage modulus, G', loss modulus, G", and complex viscosity, η*, versus angular frequency obtained through frequency sweep experiments on: (a) micellar cubic, (b) lamellar, (c) normal hexagonal, and (d) reverse hexagonal mesophases of Pluronic P84/water/p-xylene with 50/10/40, 50/35/15, 50/47.5/2.5, and 50/20/30 compositions, respectively.

A shallow minimum in G" of mesophases is a characteristic of polymeric gels and has been observed for emulsions and soft-glassy materials as well.[67,70,72–74] The minimum in loss modulus shows the presence of two relaxation behaviors in the system and the

transition from α-relaxation (long time, related to low frequency) to β-relaxation (short time, high frequency). Continuous relaxation spectra of studied samples (shown in Figure 10) are obtained from fitting the generalized Maxwell model. It is evident that the micellar cubic system has a characteristic relaxation time of $\lambda = 15.5\ s$, where the maximum in H($\lambda$) is observed. However, for lamellar, normal hexagonal, and reverse hexagonal systems, no peak is observed in the studied frequency range. Although, we can predict two relaxation times from the extrapolation of G' and G" to low and high frequencies. The longer relaxation time (>$10^2$ s) can be attributed to interfacial relaxation, while the shorter relaxation time (<$10^{-4}$ s) is related to the elasticity of water or oil in nanoconfined structures.[46]

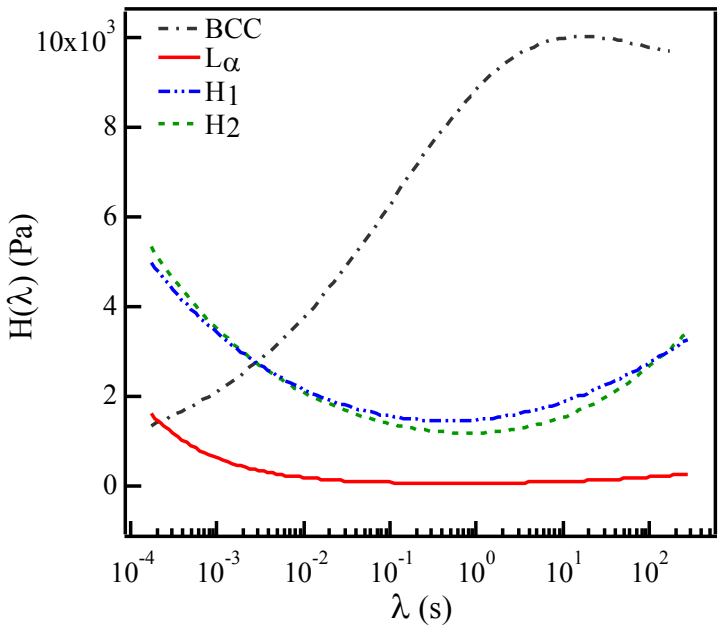


Figure 10. Continuous relaxation spectrum for micellar cubic, lamellar, normal hexagonal, and reverse hexagonal mesophase systems.

The theory of cooperative flow[64,75,76] is used to model the experimental value of moduli versus angular frequency for different mesophases. Bohlin[75] was the first one who proposed the theory of cooperative flow to correlate the microstructure of a fluid with rheology. In this theory, it is assumed that a fluid is divided into subunits where the cooperative rearrangement of subunits results in overall flow behavior. Based on this theory, the magnitude of complex modulus ($G^*$) can be expressed as a function of angular frequency ($\omega$) as follows:

$$|G^*| = \sqrt{G'(\omega)^2 + G''(\omega)^2} = A\omega^{1/z}$$

(22)

where $A$ and $z$ are the model parameters and can be obtained from fitting experimental data. $A$ is the interaction strength between flow subunits and $z$ is defined as the coordination number in the original model. Fitting parameters are summarized in Table 5. Interaction strength parameter, $A$, represents the complex viscosity at angular frequency of 1 rad/s, $|\eta^*|_{\omega=1}$.[45] Values of $|\eta^*|_{\omega=1}$ have been extracted from frequency sweep results and are listed in Table 5.

Table 5. Cooperative model fitting parameters for different mesophases and their complex viscosity at 1 rad/s.

| Structure | $A$(pa.s$^{1/z}$) | $z$ | $\eta^*_{\omega=1}$ (pa.s) |
|---|---|---|---|
| BCC | 48,874 | 11 | 48,291 |
| $L_\alpha$ | 955 | 12 | 959 |
| $H_1$ | 14,313 | 13 | 14,365 |
| $H_2$ | 16,252 | 15 | 16,201 |

Our results show that $A$ and $\eta^*_{\omega=1}$ are very close. In liquid crystal systems, Bohlin[75] suggested that $z$ is the same as the coordination number, i.e., it is equal to 2 in lamellar and 6 in hexagonal systems. However, there have been discrepancies in the reported values of $z$ in the literature. May et al.[45] observed $z$~13 for reverse hexagonal systems. Coppola et al.[28] reported a range of 5-12 for $z$ in CTAB/water mixtures for hexagonal mesophases. Rodriguez-Abreu et al. reported $z$ as 6.7 and 9.5 for reverse hexagonal and normal hexagonal mesophases, respectively.[64] It can be suggested that the $z$ value shows the average coordination number of liquid crystal grains in the polycrystalline system.

## Conclusion

Mesophases are self-assembled structures of amphiphilic molecules with the length scale in the range of 2-50 nm. Mesophases can be considered as a polycrystalline lyotropic liquid crystal, where each single crystal is oriented in a specific direction. Averaging the

elastic constant of single crystals provides the elastic modulus of polycrystalline mesophases. A mathematical model, inspired from polycrystalline metals, is proposed to estimate the elastic modulus of different mesophases as a function of their intermicellar distance. We show that the shear modulus dependence of each structure can be expressed as a function of intermicellar distance and applied deformation. Additionally, the shear modulus in the linear viscoelastic regime follows a power law dependence with the reciprocal of intermicellar distance, where the power law index for each system is different and depends on the degree of confinement. Self-assembled structures of Pluronic P84/water/p-xylene systems with 50 wt% block copolymer and different water/oil ratios are used to evaluate the accuracy of the proposed model. The results show that the model can successfully predict the order of magnitude of the elastic modulus of mesophases. Yield strain values obtained from the model are one order of magnitude higher than the experimental limits of the linear viscoelastic regime but lie in the close proximity of G'-G'' cross-over in the amplitude sweep experiment. Rheological data suggest that micellar cubic structures show a specific relaxation time of 15.5 s. The lamellar and hexagonal mesophases do not have a distinct relaxation time within the

measurement window, although two relaxation times can be predicted for them, where the longer one is attributed to the interfacial relaxation and the shorter one is related to the elasticity of solvents in nanoconfined structures. The cooperative model is successfully used to fit the frequency sweep data of mesophase systems.

## Electronic Supplementary Information

Derivation of elastic constants for different mesophase systems can be found in the Electronic Supplementary Information.

## Conflicts of Interest

There are no conflicts to declare.

## Acknowledgement

The authors thank Aaron Lindsay for assistance with SAXS measurements and Elijah Wade for helpful discussions. This work was supported in part by U.S. Department of the Interior, Bureau of Reclamation (Agreement No. R16AC0002). This work was performed in part at the Center for Integrated Nanotechnologies (CINT) at the Los Alamos National Laboratories (LANL). CINT is funded by the DOE Office of Basic Energy Sciences. LANL is operated by Los Alamos National Security, LLC, for the National Nuclear Security

Administration of the U.S. Department of Energy under contract DE-AC52-06NA25396. S.Q. and R.F. thank National Science Foundation (award No. 1438584) that made the purchase of the rheometer possible.

## References

1 J. Du and R. K. O'Reilly, *Soft Matter*, 2009, **5**, 3544–3561.

2 D. U. Ahn and E. Sancaktar, *Soft Matter*, 2008, **4**, 1454–1466.

3 P. Alexandridis and B. Lindman, *Amphiphilic block copolymers: self-assembly and applications*, Elsevier, 2000.

4 J. Liu, a. Y. Y. Kim, L. Q. Q. Wang, B. J. J. Palmer, Y. L. L. Chen, P. Bruinsma, B. C. C. Bunker, G. J. J. Exarhos, G. L. L. Graff, P. C. C. Rieke, G. E. E. Fryxell, J. W. W. Virden, B. J. J. Tarasevich and L. a. A. Chick, *Adv. Colloid Interface Sci.*, 1996, **69**, 131–180.

5 P. Alexandridis, U. Olsson and B. Lindman, *Macromolecules*, 1995, **28**, 7700–7710.

6 P. Holmqvist, P. Alexandridis and B. Lindman, *Langmuir*, 1997, **13**, 2471–2479.

7 P. Alexandridis, U. Olsson and B. Lindman, *Langmuir*, 1997, **13**, 23–34.

8 P. Alexandridis, U. Olsson and B. Lindman, *Langmuir*, 1998, **14**, 2627–2638.

9 L. Yang and P. Alexandridis, *Curr. Opin. Colloid Interface Sci.*, 2000, **5**, 132–143.

10 O. Parisi, L. Scrivano, S. Candamano, M. Ruffo, A. Vattimo, M. Spanedda and F. Puoci, *Molecules*, 2017, **23**, 63.

11 N. A. Gujarathi, B. R. Rane and R. K. Keservani, in *Novel Approaches for Drug Delivery*, Medican Information Science Reference, 2017, pp. 190–216.

12 S. Hocine and M.-H. Li, *Soft Matter*, 2013, **9**, 5839–5861.

13 L. Sievens-figueroa and C. A. Guymon, *Chem. Mater.*, 2009, **21**, 1060–1068.

14 D. T. McCormick, K. D. Stovall and C. A. Guymon, *Macromolecules*, 2003, **36**, 6549–6558.

15 M. A. DePierro, K. G. Carpenter and C. A. Guymon, *Chem. Mater.*, 2006, **18**, 5609–5617.

16 M. Zhou, P. R. Nemade, X. Lu, X. Zeng, E. S. Hatakeyama, R. D. Noble and D. L. Gin, *J. Am. Chem. Soc.*, 2007, **129**, 9574–9575.

17 X. Feng, M. E. Tousley, M. G. Cowan, B. R. Wiesenauer, S. Nejati, Y. Choo, R. D. Noble, M. Elimelech, D. L. Gin and C. O. Osuji, *ACS Nano*, 2014, **8**, 11977–11986.

18 H.-P. Hentze and E. W. Kaler, *Curr. Opin. Colloid Interface Sci.*, 2003, **8**, 164–178.

19 S. Qavi, A. Lindsay, M. Firestone and R. Foudazi, *J. Memb. Sci.*, 2019, **580**, 125–133.

20 F. Kleitz, T. Czuryszkiewicz, A. Leonid A. Solovyov and M. Lindén, *Chem. Mater.*, 2006, **18**, 5070–5079.

21 F. Kleitz, A. Tae-Wan Kim and R. Ryoo, *Langmuir*, 2005, **22**, 440–445.

22 R. Jiaxiang, S. S. Adriana and R. Krishnamoorti, *Macromolecules*, 2000, **33**, 3739–3746.

23 J. M. Sebastian, C. Lai, W. G. William and A. R. Richard, *Macromolecules*, 2002, **35**, 2707–2713.

24 M. B. Kossuth, D. C. Morse and F. S. Bates, *J. Rheol.*, 1998, **43**, 167–196.

25 G. Palazzo, *Soft Matter*, 2013, **9**, 10668–10677.

26 K. Morishima, S. Sugawara, T. Yoshimura and M. Shibayama, *Langmuir*, 2017, **33**,

6084–6091.

27 G. Montalvo, M. Valiente and E. Rodenas, *Langmuir*, 1996, **12**, 5202–5208.

28 L. Coppola, R. Gianferri, I. Nicotera, C. Oliviero and G. A. Ranieri, *Phys. Chem. Chem. Phys.*, 2004, **6**, 2364–2372.

29 A. A. Adams, M. J. Solomon, R. G. Larson and X. Xia, *J. Rheol.*, 2017, **61**, 967–977.

30 X. Li, E. Park, K. Hyun, L. Oktavia and M. Kwak, *J. Rheol.*, 2018, **62**, 107–120.

31 I. W. Hamley, *Curr. Opin. Colloid Interface Sci.*, 2000, **5**, 341–349.

32 I. W. Hamley and V. Castelletto, *Prog. Polym. Sci.*, 2004, **29**, 909–948.

33 N. P. Balsara and B. Hammouda, *Phys. Rev. Lett.*, 1994, **72**, 360.

34 I. Hamley, in *Block Copolymers in Solution: Fundamentals and Applications*, Wiley Online Library, 2012, pp. 105–172.

35 J. Zipfel, J. Berghausen, G. Schmidt, P. Lindner, P. Alexandridis and W. Richtering, *Macromolecules*, 2002, **35**, 4064–4074.

36 J. Zipfel, J. Berghausen, G. Schmidt, P. Lindner, P. Alexandridis, M. Tsianou and

W. Richtering, *Phys. Chem. Chem. Phys.*, 1999, **1**, 3905–3910.

37 J.-P. Habas, E. Pavie, A. Lapp and J. Peyrelasse, *Rheol. Acta*, 2008, **47**, 765–776.

38 K. Van Workum and J. J. de Pablo, *Phys. Rev. E*, 2003, **67**, 031601.

39 A. A. Joshi, J. K. Whitmer, O. Guzmán, N. L. Abbott and J. J. de Pablo, *Soft Matter*, 2014, **10**, 882–893.

40 K. Van Workum and J. J. de Pablo, *Phys. Rev. E*, 2003, **67**, 011505.

41 D. N. Blaschke, *J. Appl. Phys.*, 2017, **122**, 145110(1-6).

42 D. Tromans, *Int. J. Res. Rev. Appl. Sci.*, 2011, **6**, 462–483.

43 G. R. Barsch, *J. Appl. Phys.*, 1968, **39**, 3780–3793.

44 J. M. J. den Toonder, J. A. W. van Dommelen and F. P. T. Baaijens, *Model. Simul. Mater. Sci. Eng.*, 1999, **7**, 909–928.

45 A. May, K. Aramaki and J. M. Gutiérrez, *Langmuir*, 2011, **27**, 2286–2298.

46 R. Mezzenga, C. Meyer, C. Servais, A. I. Romoscanu, L. Sagalowicz and R. C. Hayward, *Langmuir*, 2005, **21**, 3322–3333.

47 L. Sagalowicz, R. Mezzenga and M. E. Leser, *Curr. Opin. Colloid Interface Sci.*, 2006, **11**, 224–229.

48 J. F. Nye, *Physical properties of crystals : their representation by tensors and matrices*, Clarendon Press, 1985.

49 W. Voigt, *Ann. Phys.*, 1889, **274**, 573–587.

50 S. L. Deore and S. N. Kale, *Syst. Rev. Pharm.*, 2017, **8**, 39–47.

51 M. K. SHARMA and D. O. SHAH, in *ACS Symposium Series*, American Chemical Society , 1985, pp. 1–18.

52 R. Goetz, R. Lipowsky and R. Diger Goetz, *J. Chem. Phys.*, 1998, **108**, 7397–7409.

53 W. Callister and D. Rethwisch, *Materials Science and Engineering, an Introduction*, John Wiley & Sons, 8th editio., 2014.

54 J. N. Israelachvili, *Intermolecular and Surface Forces.*, Academic, London, 1992.

55 J. R. Barber, *Elasticity*, Springer, 2010.

56 B. A. Smith, E. T. Samulski, L.-P. Yu and M. A. Winnik, *Phys. Rev. Lett.*, 1984, **52**, 45–48.

57 A. K. Fritzsche and F. P. Price, *Polym. Eng. Sci.*, 1974, **14**, 401–412.

58 B. W. Henry and B. W. Lawrence, *Proc. R. Soc. London. Ser. A, Contain. Pap. a Math. Phys. Character*, 1913, **88**, 428–438.

59 P. Alexandridis, U. Olsson and B. Lindman, *J. Phys. Chem.*, 1996, **100**, 280–288.

60 J. Lauger, R. Linemann and W. Richtering, *Rheol. Acta*, 1995, **34**, 132–136.

61 M. Lukaschek, D. A. Grabowski and C. Schmidt, *Langmuir*, 1995, **11**, 3590–3594.

62 Q. Chang and Q. Chang, *Colloid Interface Chem. Water Qual. Control*, 2016, 79–136.

63 C. Daniel, I. W. Hamley, M. Wilhelm and W. Mingvanish, *Rheol. Acta*, 2001, **40**, 39–48.

64 C. Rodriguez-Abreu, D. P. Acharya, K. Aramaki and H. Kunieda, *Colloids Surfaces A Physicochem. Eng. Asp.*, 2005, **269**, 59–66.

65 I. Masalova, A. Y. Malkin and R. Foudazi, *Appl. Rheol.*

66 R. Foudazi, S. Qavi, I. Masalova and A. Y. Malkin, *Adv. Colloid Interface Sci.*, 2015, **220**, 78–91.

67 R. Foudazi, I. Masalova and A. Y. Malkin, *J. Rheol.*, 2012, **56**, 1299–1314.

68 K. Hyun, S. H. Kim, K. H. Ahn and S. J. Lee, *J. Nonnewton. Fluid Mech.*, 2002, **107**, 51–65.

69 N. Phan-Thien, M. Safari-Ardi and A. Morales-Patino, *Rheol. Acta*, 1997, **36**, 38–48.

70 T. Mason, J. Bibette and D. Weitz, *Phys. Rev. Lett.*, 1995, **75**, 2051–2054.

71 T. Mason and D. Weitz, *Phys. Rev. Lett.*, 1995, **75**, 2770–2773.

72 R. J. Ketz, R. K. Prud'homme and W. W. Graessley, *Rheol. Acta*, 1988, **27**, 531–539.

73 M. Laurati, G. Petekidis, N. Koumakis, F. Cardinaux, A. B. Schofield, J. M. Brader, M. Fuchs and S. U. Egelhaaf, *J. Chem. Phys.*, 2009, **130**, 134907.

74 P. Sollich, *Phys. Rev. E*, 1998, **58**, 738–759.

75 L. Bohlin, *J. Colloid Interface Sci.*, 1980, **74**, 423–434.

76 D. Gabriele, B. de Cindio and P. D'Antona, *Rheol. Acta*, 2001, **40**, 120–127.

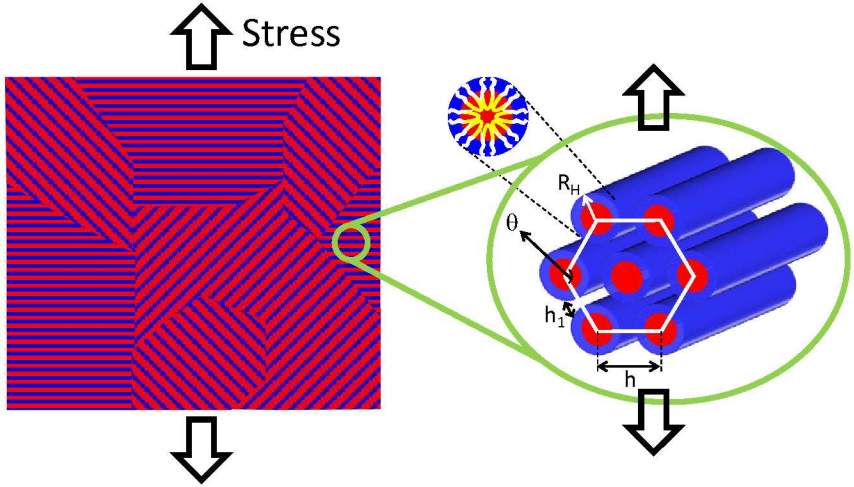
Stress
$R_H$
θ
$h_1$
h

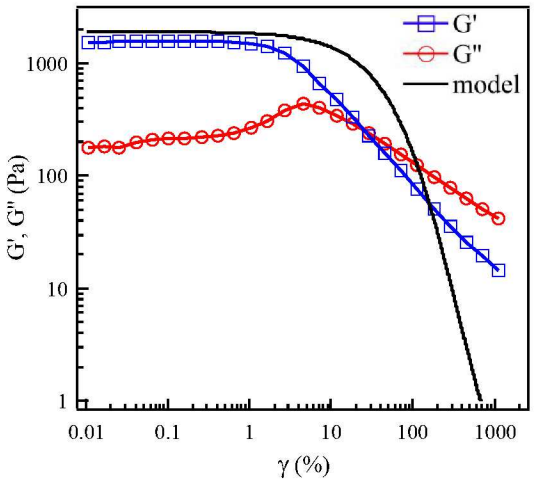
G'
G"
model
1000
100
10
1
G', G" (Pa)
0.01
0.1
1
10
100
1000
γ (%)